

A Numerical Study on Bank Erosion of a Braided Channel: Case study of the “Tangail and Manikganj Districts along the Brahmaputra River”

Islam Md Masbahul*
MEE19713

Supervisors: Dr. Atsuhiko Yorozuya **
Professor Shinji Egashira ***
Dr. Daisuke Harada ****

ABSTRACT

This study aims to predict the vulnerable location of bank erosion along the braided river, which is composed of many different channels. For this study, the authors paid attention to two aspects. The first point is changing of flow discharge along the channel, which belongs to the area of interest as a large-scale phenomenon. The second point is changing the geometry by the sand bar and the changing of the flow associated with it as a small-scale phenomenon.

The large-scale phenomenon is important since increasing discharge indicates increasing not only bank erosion but all the vulnerabilities associated with it. To consider the two different scales, the authors determine the domain as an entire channel. By using numerical simulation and satellite data analysis the two-scale phenomena were described. Regarding the large-scale phenomenon, the morphology and the channel change pattern were evaluated and regarding the small-scale phenomenon, the vulnerable location of bank erosion was predicted.

Finally, the author proposed the fixing of existing countermeasures by adding future predictions.

Keywords: Braided Channel, Bank erosion, Numerical simulation, Bed deformation, Channel bifurcation.

INTRODUCTION

The Brahmaputra is categorized as the largest braided, suspended sediment dominated, and most erosion-prone river in Bangladesh (Biswas, 2016 and GUL, 2019). The temporal and spatial variations of the braided river channels are related to flow discharge. The increase in flow discharge is a large-scale phenomenon that affects both local bank erosion and the sediment transport rate, exacerbating flooding. More than 60% of affected people live on the floodplain of the Brahmaputra River (Biswas, 2016) and local bank erosion causes a loss of thousands of hectares of agricultural land, in addition to buildings, mosques, roads, etc. each year. Burger et al. (1988), Ashworth et al. (2000), and Best et al. (2008) analyzed Brahmaputra river bank erosion based on satellite images. Their studies show that the Brahmaputra River's annual bank erosion rate in Bangladesh is on the order of 10^2 to 10^3 ha per year. Severe river bank erosion occurs from July to September (BWDB, 2018), and the Bangladesh Water Development Board (BWDB) implements temporary emergency countermeasures at the erosion points. Because of the river's high-water level and the scarcity of labor and materials, conducting emergency countermeasures during floods is costly and ineffective. Therefore, it is very important to predict the vulnerable locations of bank erosion to take countermeasures earlier.

The Center for Environmental and Geographic Information Services (CEGIS) is one of the leading organizations in Bangladesh that predicts bank erosion of major rivers based on the analysis of satellite

* Sub-Divisional Engineer, Bangladesh Water Development Board (BWDB), Bangladesh.

** Associate Professor at National Graduate Institute for Policy Studies (GRIPS), and senior researcher at International Center for Water Hazard and Risk Management (ICHARM), Public Works Research Institute (PWRI), Japan.

*** Dr. Eng., Professor at GRIPS, of ICHARM, PWRI, Japan.

**** Research specialist, Water-related hazard group, ICHARM, Japan.

images and probabilistic approaches (CEGIS, 2020). In addition to satellite image analysis, numerical simulation is an important tool for identifying the vulnerable locations of bank erosion.

To predict the vulnerable locations of bank erosion by numerical simulation, the development of initial river morphology is very important where observational bathymetry data is not available. In the current study, the author developed the initial river morphology based on the relationship between the inundation area and the water depth, using time-series satellite images and observed water level data. To find vulnerable bank erosion points using numerical simulation, it is important to understand the channel bifurcation process and the effect of the increase in discharge on local bank erosion. The author conducted a numerical simulation for the morphological assessment before conducting a numerical simulation of bank erosion. The vulnerable locations found from the simulation results were validated by the analysis of satellite images before and after the flood. Finally, the author proposed some temporal countermeasures to take in advance at vulnerable locations, to save both land and infrastructure from river erosion.

THEORY AND METHODOLOGY

The governing equations used in the numerical simulation are as follows:

$$\text{Mass Conservation: } \frac{\partial h}{\partial t} + \frac{\partial uh}{\partial x} + \frac{\partial vh}{\partial y} = 0 \quad (1)$$

$$\text{Momentum Conservation: x-component } \frac{\partial uh}{\partial t} + \frac{\partial uuh}{\partial x} + \frac{\partial uvh}{\partial y} = -gh \frac{\partial(h+z_b)}{\partial x} - \frac{\tau_x}{\rho} + \frac{1}{\rho} \left(\frac{\partial h \tau_{xx}}{\partial x} + \frac{\partial h \tau_{yx}}{\partial y} \right) \quad (2)$$

$$\text{Momentum Conservation: y-component } \frac{\partial vh}{\partial t} + \frac{\partial vuh}{\partial x} + \frac{\partial vvh}{\partial y} = -gh \frac{\partial(h+z_b)}{\partial y} - \frac{\tau_y}{\rho} + \frac{1}{\rho} \left(\frac{\partial h \tau_{xy}}{\partial x} + \frac{\partial h \tau_{yy}}{\partial y} \right) \quad (3)$$

Where, h is the flow depth; u and v are the x and y components of depth-average velocity; t is the time; g is the acceleration due to gravity; ρ is the mass density of water; τ_{xx} , τ_{yy} , τ_{xy} and τ_{yx} are the depth-averaged Reynolds stresses; and τ_x and τ_y are the x and y components of the bed shear stress, respectively. Bed shear stress can be expressed as:

$$\frac{\tau_b}{\rho} = \frac{n^2 g}{h^{\frac{1}{3}}} (u^2 + v^2) \quad (4)$$

Where, τ_b is the bed shear stress and n is the Manning's roughness coefficient. For bed load conditions, Egashira et al. (1991) proposed a non-dimensional bed load as the 2.5th power of non-dimensional bed shear stress based on the constitutive relation of the solid particle–water mixture. The equation is expressed as follows:

$$q_{b*} = \frac{4}{15} \frac{K_1^2 K_2}{\sqrt{f_d + f_f}} \tau_*^{5/2} \quad (5)$$

where, K_1 , K_2 , f_d and f_f are specified theoretically. For the suspended load case, the particle entrainment from the bed layer to suspension occurs when the particle's upward velocity is greater than its fall velocity (Figure 1). The depth-integrated mass conservation equation of suspended sediment can be expressed as:

$$\frac{\partial \bar{c}h}{\partial t} + \frac{\partial r_1 \bar{c}uh}{\partial x} + \frac{\partial r_1 \bar{c}vh}{\partial y} = \frac{\partial}{\partial x} (h \epsilon_x \frac{\partial \bar{c}}{\partial x}) + \frac{\partial}{\partial y} (h \epsilon_y \frac{\partial \bar{c}}{\partial y}) + E - D \quad (6)$$

Where \bar{c} , \bar{u} and \bar{v} are the average values for sediment concentration, x -component of velocity, and y -component of velocity, ϵ_x and ϵ_y are the x and y -component of dispersion coefficient (similar to turbulent diffusion coefficient), h is the flow depth, E is the erosion rate of sediment, D is the deposition rate and r_l is the correction factor. For the computation of erosion term of the above equation, Harada et al. (2019) proposed the equation of entrainment velocity as follows:

$$\frac{W_e}{V} = \frac{K}{R_{i*}}, (R_{i*} = \frac{\Delta \rho}{\rho} gh/V^2), K = 1.5 \times 10^{-3}, c_e = \frac{W_e}{w_0} c_s, V = \sqrt{u^2 + v^2} \quad (7)$$

Where $K = 1.5 \times 10^{-3}$, w_0 is the fall velocity, w_e is the entrainment velocity, c_s is the sediment concentration at the surface layer, c_e is the equivalent sediment concentration, h is the flow depth, and ρ is the mass density of water. For uniform sediment particle size, the temporal change in river bed variation can be evaluated by applying continuity of mass condition of bed sediment, which can be expressed as:

$$\frac{\partial z_b}{\partial t} + \frac{1}{\lambda-1} \left(\frac{\partial q_{bx}}{\partial x} + \frac{\partial q_{by}}{\partial y} + E_s - D_s \right) = 0 \quad (8)$$

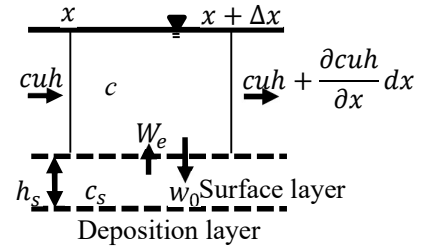


Figure 1: Particle Entrainment Model

Where, z_b is the river bed elevation; q_{bx} and q_{by} are the components of bedload transport rate in the x and y directions, respectively; E_s is the erosion rate; and D_s is the sediment deposition rate.

For bank erosion, the temporal change of riverbed variation is evaluated by equation (8), if $\frac{\partial z_b}{\partial t} < 0$ bank shifting is computed as $\frac{\partial B}{\partial t} = \alpha u_*$ again, $\frac{\partial z_b}{\partial t}$ is computed, so that the mass of $\frac{\partial B}{\partial t} = \frac{\partial z_b}{\partial t} \frac{1}{dy}$ Where, B is the channel width, u_* is the shear velocity, and $\alpha = 0.005$.

DATA

A fundamental relationship between the inundation area and water depth has been employed to develop the river's initial morphology. As the river discharge increases, the water level also increases; therefore, more areas surrounding the river are inundated. The increase and decrease of the inundated area concerning water level change can be marked in time-series satellite images. To obtain river bathymetry, the water area was marked in the time series USGS Landsat satellite images, then the images were superimposed. The observed cross-section and the formula proposed by Yorozuya et al. (2013) were used to obtain the channel shape below the lowest water level. The formula explains how the flow depth of a river changes as the width of the river changes. Initial morphology of the year 2010, 2014, 2018 and 2019 were developed using this technique. For the numerical simulation of morphology evaluation, in the upstream boundary, unsteady flow discharges of 2011 and 2015 were used to simulate the initial conditions of the year 2010 and 2014. For the numerical simulation of bank erosion, the author used a flood discharge of 65,000 m³/s. Discharge of 65,000 m³/s was obtained from the statistical analysis of a 10-year return period. The following calculation conditions were used in the numerical simulation.

Study area: 65 × 12 km, grid size: 100 m × 100 m, time step (dt): 0.5 second, particle size: 0.25 mm, Manning's roughness: 0.025, River bed slope: 0.00007

RESULTS AND DISCUSSION

Results of the Morphological Evaluation

Figure 2 shows a comparison of the simulated and observed channel patterns. Figure 2 (a) and (b) show the observed (digitized image of USGS Landsat) and simulated (2010 initial condition) channel patterns after the 2011 flood. Similarly, Figure 2 (c) and (d) show the observed (digitized image of USGS Landsat) and simulated (2014 initial condition) channel patterns after the 2015 flood. In both simulations, the multiple row bars and sandbar patterns are very similar to the observed pattern.

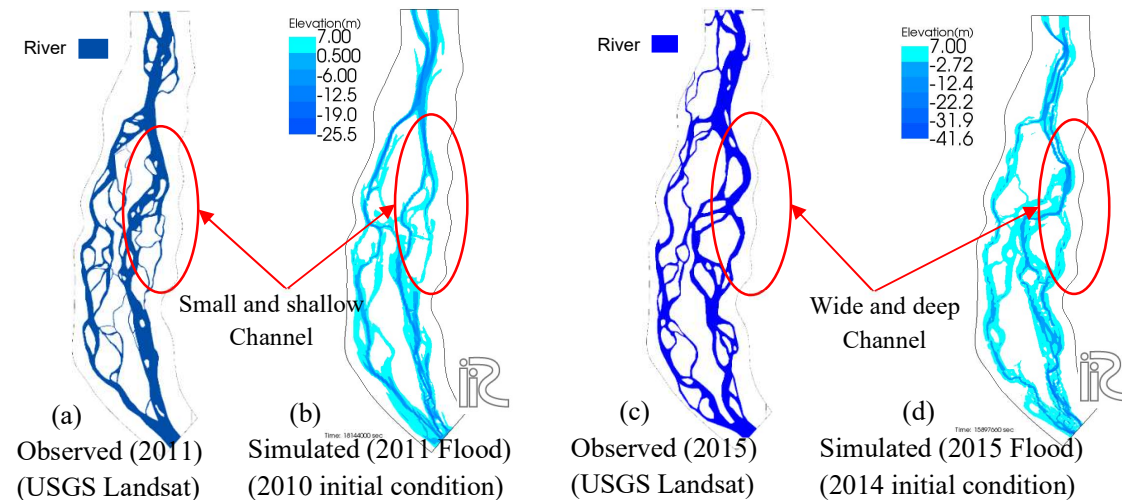


Figure 2: Comparison of simulated channel pattern with observed (USGS Landsat)

The simulated results can be assessed in terms of channel pattern and sandbar formation. After the 2011 flood, both the observed and simulated results show that the left channel is small and shallow (red circle in Figure 2 (a) and (b)). However, after the 2015 flood, the left channel (red circle in Figure 2 (c) and (d)) is wide and deep. Such morphological changes occur due to the increased discharge in the left channel, as shown in Figure 3.

Figure 3 shows how an increase in discharge in the left channel lead to the channel bifurcation process. Figure 3 (a) and (b) show the channel depth after the flood simulation of the year 2011 and 2015. After the 2015 flood, the left channel became deeper and wider. Figure 3 (c) shows the simulated discharge in the left and right channels for both the floods of 2011 and 2012. During the 2011 simulated flood, we observed a small difference in discharge between the left and right channels. Such a small difference in discharge between the two channels creates a difference in the shear velocity and sediment supply in the channels. As a result, some blockage or appearance of the sandbar occurs in the channel, which leads to the channel bi-furcation process. Because of this process, one channel becomes stronger than the other channel. During the 2012 flood (Figure 3 (c)), the difference between the left and right channel discharge increased by 30% (at peak discharge) compared to the 2011 flood. From the simulated discharge of the 2015 flood (Figure 3 (d)), we can see that the left channel carries most of the flow (70% at peak flood) than the right channel.

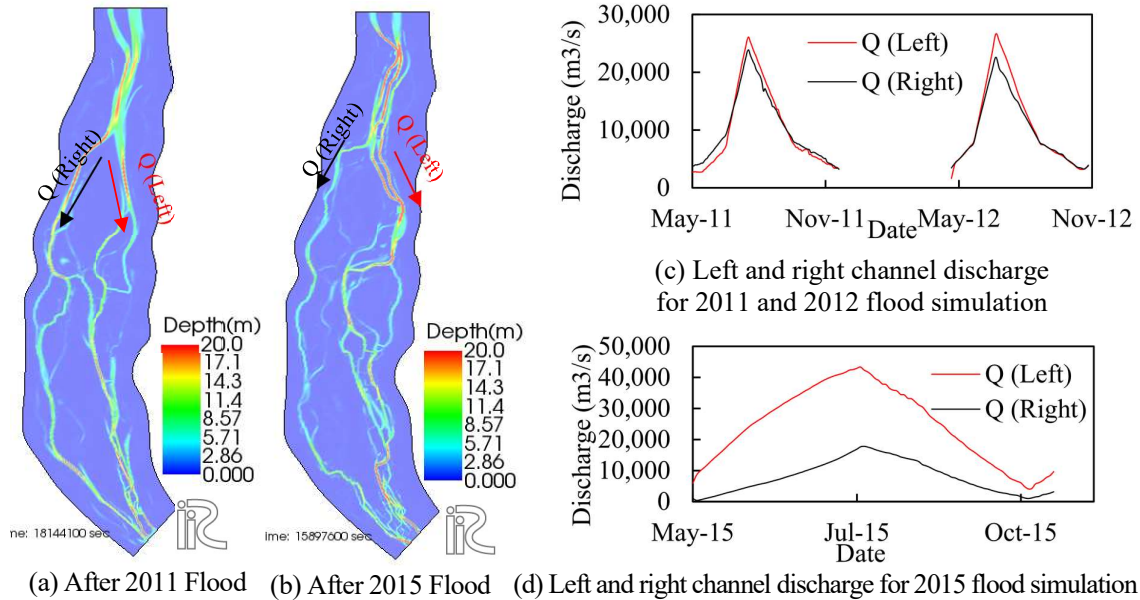


Figure 3: Channel bifurcation process

Comparing the simulated channel patterns (Figure 2 (b) and (d)) and channel depth (Figure 3 (a) and (b)) after the flood of 2011 and 2015, we can say that the left channel became wider and deeper during the flood because it carried more discharge. Therefore, the vulnerability of the left channel increased as the discharge increased, and such vulnerability led to local bank erosion.

Results of the Bank Erosion Simulation

Since the vulnerability increases as the discharge increases in the channel, to conduct numerical simulation of bank erosion, a steady flow of $65,000 m^3/s$ discharge (10-year return period) was used for the initial morphology of the year 2018 as shown in Figure 4 (a). Figure 4 (c) shows the location of the simulated bank erosion after 60 days of simulation. Figure 4 (b) shows the observed bank erosion in 2019 (digitizing from the USGS Landsat image). The results show that the simulated bank erosion pattern is very similar to the observed bank erosion (marked by circles). Figure 4 (d) compares the observed bank erosion and simulated bank erosion along the left bank. From the comparison, we can see that our simulation underestimates the bank erosion by 2 to 3 times the observed erosion. This can be investigated in terms of suspended sediment concentration with non-uniform particle size. However, from the simulated result, we can obtain the vulnerable locations of bank erosion.

The validity of our simulated results can be justified by analyzing the satellite images before and after the flood. Figure 5(a) and (b) show the satellite images before and after the 2018 flood. The three sand bars were separated before the flood (Figure 5(a)), and each flow was divided into two parts before hitting the sandbars. During the flood, the sand bars merged (Figure 5(b)) and the flow velocity directly hit the bank, causing bank erosion. A similar explanation is found in the simulation results. Figure 5(d) shows the result after 60 days, where the sandbars merged and the concentrated flow hit the bank. Therefore, the vulnerability of bank erosion can be expressed in terms of the sudden appearance of sand bars, increase in flow discharge, and the direction of flow properties. Based on the numerical simulations and analysis of satellite images, the vulnerable locations of bank

erosion can be predicted. Analysis of satellite images shows that if temporal countermeasures are taken before the flood, then 200 ha to 400 ha of land can be saved from bank erosion each year.

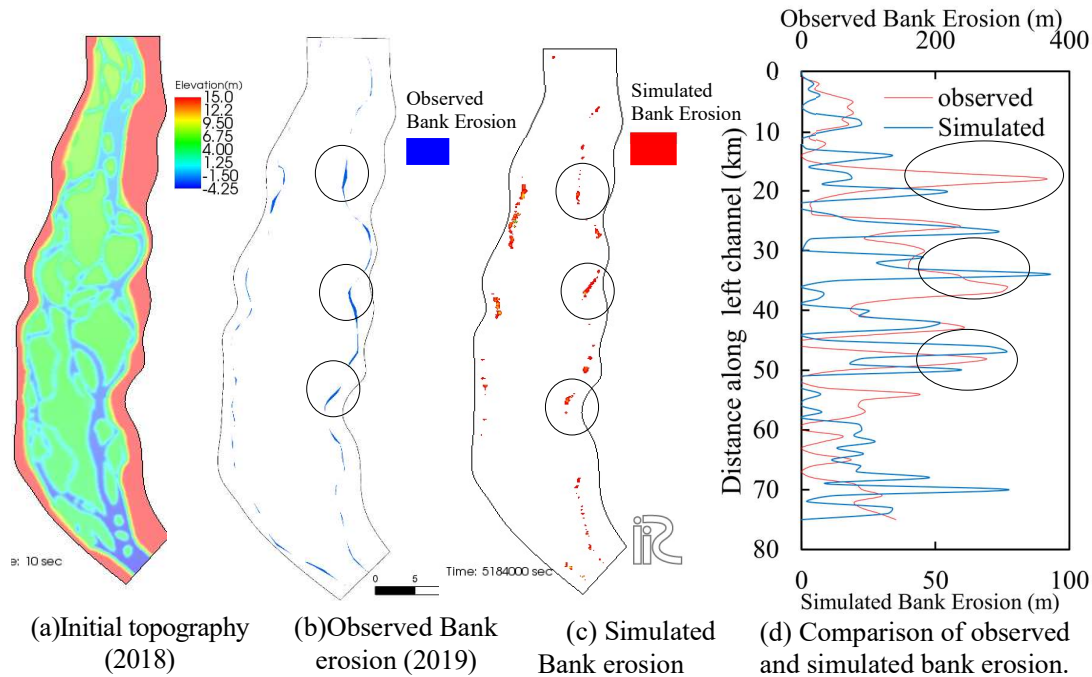


Figure 4: Bank erosion result comparison

CONCLUSIONS

The present study aims to understand the channel development process and predict the vulnerable locations of bank erosion. The results obtained from the numerical simulation with the actual floods of 2011 and 2015 suggest that our simulation can reproduce channel shape and sandbar patterns that are very close to the observed ones. From the simulation results, it is clear that a small difference in discharge between the two channels creates instability in terms of blockage by a sandbar, and such instability leads to the channel bi-furcation process. As a result, one channel becomes dominant and carries more discharge than the other. The result of the bank erosion model suggests that our simulation can predict the vulnerable locations of bank erosion.

RECOMMENDATION

Table 1 shows an overall summary of the activities during a target year that can be applied to reduce land loss from bank erosion. The observed data of BWDB shows that flooding occurs in the Brahmaputra River from June to October. To take countermeasures in a target year, the necessary data needs to be collected after the flood of target year-1 from November to December. For example, if we want to take countermeasures in 2021, we need to collect the necessary data from November to December of 2020. In January, based on numerical simulation results and satellite image analysis, we will have vulnerable locations of bank erosion for the target year. From February to May, we can apply temporal countermeasures at vulnerable locations. The temporal countermeasures may include suggesting farmers

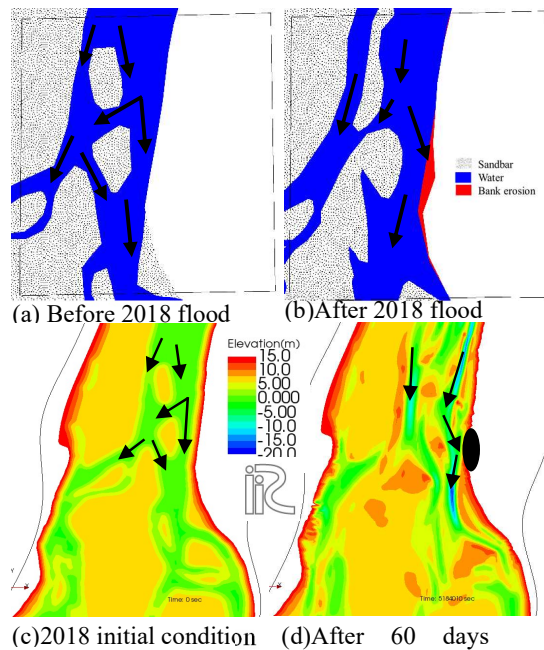


Figure 5: Bank erosion process

harvest early, construction of a bamboo/wooden spur, dumping of sand-filled geotextile bags, etc., as per the design and specification of BWDB. The activities explained in Table 1 can be repeated for the countermeasures of the following target year. The temporal countermeasures on any specific vulnerable point can be continued for at most three target years. During the time of temporal countermeasures, detailed data (geomorphological, hydrological, economic, etc.) of vulnerable locations needs to be collected to prepare the project proposal of permanent countermeasures for vulnerable locations.

Table 1: Summary of activities for temporal countermeasures

Year	Timeline	Objective	Activities
Target year-1	Nov-Dec	To Find Vulnerable Locations	Develop initial boundary conditions: Develop initial river morphology using the proposed technique, collect field data.
Target year	Jan		Conduct numerical simulation (as explained in Figure 2 and Figure 3) Satellite image analysis (as explained in Figure 4 and Figure 5)
Target year	Feb-May	To Protect Land and Infrastructure from Erosion	Temporal Countermeasure: Construct a bamboo/wooden spur, dumping of sand-filled geotextile bags, etc. as per the design and specification of BWDB.

ACKNOWLEDGEMENTS

I would like to express my sincere thanks to my Supervisors, Associate Professor Atsuhiko Yorozuya, Professor Shinji Egashira, and Dr. Daisuke Harada for their knowledge, guidance, and supervision during the entire period of my research. The author would also like to express his profound indebtedness to Dr. Robin Kumar Biswas, a research assistant, for his active and continuous mental support. I want to thank the JICA and ICHARM staff for their support and help during my studies and stay in Japan. Finally, the author would like to express his earnest gratitude to his parents and wife for their continuous inspiration and mental support to complete the study.

REFERENCES

- Ashworth, P.J; Best, J.L; Roden, J.E; Bristow, C.S; Kallassen, G. (2000). Morphological evolution and dynamics of a large, sand braid-bar, Jamuna River, Bangladesh. *International Association of Sedimentologists, Sedimentology*, 47, 533–555.
- Best, JL; Ashworth, P.J; Sarker, M.H; Roden, J. (2008). The Brahmaputra-Jamuna River, Bangladesh. In *Large Rivers: Geomorphology and Management*. <https://doi.org/10.1002/9780470723722.ch19>
- Biswas, R. K. (2016). *Numerical prediction of channel changes in large, braided rivers dominated by suspended sediment*.
- Burger, J.W; Klaassen, G.J; Prins, A. (1988). Bank erosion and channel processes in the Jamuna River, Bangladesh. *International Symposium on the Impact of River Bank Erosion, Flood Hazards and the Problem of Population Displacement, Dhaka, Bangladesh, April 11-13*.
- BWDB. (2018). *ANNUAL FLOOD REPORT 2018*.
- CEGIS. (2020). *PREDICTION OF RIVERBANK EROSION 2020 (JAMUNA, GANGES AND PADMA RIVERS)*. <https://www.cegisbd.com/EventData?Evntid=36>
- Egashira, S.; Ashida, K.; Anonaka, S.; & Takahashi, T. (1991). Bed-load formula derived from constitutive equations of solid particle–water mixture. *Bull Disas Prev Res Inst, Kyoto Univ, Japan*, 34(B), 261.
- GUL, A. Al. (2019). *Fundamental study for 2-D numerical simulation of channel changes in large rivers dominated by fine sediment*.
- Harada, D.; Egashira, S.; Ahmed, T.S.; Katayama, N. (2019). Erosion Rate of Bed Sediment by means of Entrainment Velocity. *Journal of Japan Society of Civil Engineers*, 75(4).
- Yorozuya, A; Islam, M.S; Kamoto, M; Egashira, S. (2013). Influence of Jamuna Bridge on river morphology. *Advances in River Sediment Research*.